ACS APPLIED POLYMER MATERIALS

pubs.acs.org/acsapm

Article

Functional Poly(ε-caprolactone)/Poly(ethylene glycol) Copolymers with Complex Topologies for Doxorubicin Delivery to a Proteinase-Rich Tumor Environment

Wanda Celentano,[#] Marco Pizzocri,[#] Filippo Moncalvo, Federico Pessina, Michela Matteoli, Francesco Cellesi,[*,#] and Lorena Passoni[*,#]

Cite This: *ACS Appl. Polym. Mater.* 2022, 4, 8043−8056

Read Online

ACCESS | Metrics & More | Article Recommendations | Supporting Information

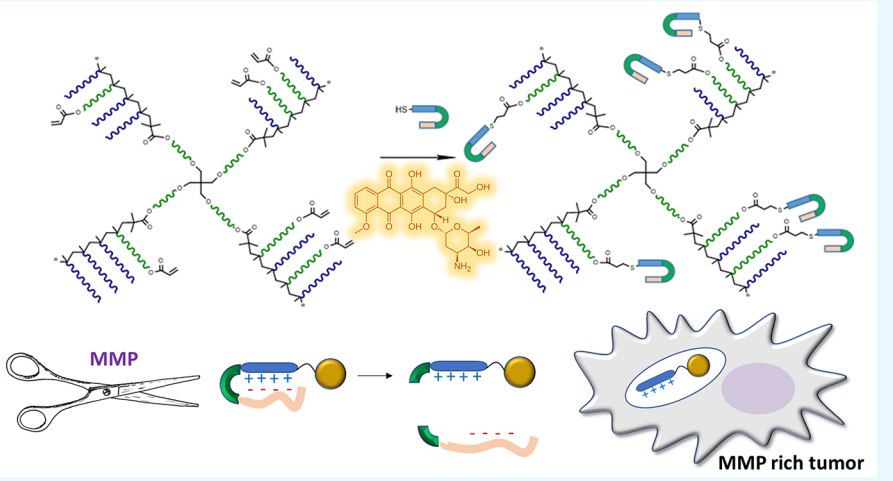

ABSTRACT: Doxorubicin (DOX)-loaded polymer nanoparticles based on poly(ethylene glycol)-poly(ε-caprolactone) copolymers with a complex macromolecular topology are proposed to tackle the matrix metalloproteinase (MMP)-rich tumor environment. Linear, 4-arm comb-like copolymers and 4-arm brush block copolymers were synthesized through a combination of ring opening polymerization and atom transfer radical polymerization, in order to control the molar mass distribution, the arm/brush architecture, as well as the final size and DOX loading of self-assembled nanoparticles obtained by nanoprecipitation. The optimized nanocarriers were conjugated with penetrating low molecular weight protamine peptides coupled to a polyanionic inhibitory domain cleavable by matrix metalloproteinase-2 (MMP2). DOX-loaded, MMP2-activable nanocarriers were evaluated in the context of glioblastoma (GBM), a brain tumor characterized by remarkable and relevant MMP2 expression. Uptake and cytotoxicity in patient-derived GBM cells correlated with the level of MMP2 enzymatic activity in a dose- and time-dependent manner. No effects were observed in nontumoral endothelial cells that do not express MMP2. Results demonstrated that, by tuning polymer topology and peptide sequence, nanoparticle self-assembly, DOX encapsulation, and delivery can be optimized for the development of an advanced treatment for MMP2-overexpressing tumors.

KEYWORDS: *polymer nanoparticles, complex architecture, doxorubicin, matrix metalloproteinase, penetrating peptide, glioblastoma*

INTRODUCTION

Nanoparticles (NPs) and micelles based on amphiphilic block copolymers have attracted significant attention in nanomedicine and drug delivery,[1,2] particularly in cancer treatments to enhance drug solubilization, stabilization, and targeting.[3−6] Recently, block copolymers based on poly(ε-caprolactone) (PCL) and PEG have been investigated as efficient drug nanocarriers.[7,8] PCL guarantees biocompatibility, biodegradability and the formation of a hydrophobic nanoparticle core required to entrap chemotherapeutic drugs and exceed their solubility thresholds in aqueous solutions. The hydrophilic PEG block provides colloidal stability, a stealth characteristic for circulation enhancement in blood, thus improving pharmacokinetic profiles and therapeutic efficacy.[9,10]

Received: May 26, 2022
Accepted: September 29, 2022
Published: October 13, 2022

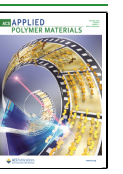

While medical products based on PEG and PCL have reached market approval from regulatory authorities,[8] PEG-PCL NPs are well tolerated both *in vitro* and *in vivo*.[7,8,11] No acute toxic side effects were detected after single or multiple dosing in experimental animals,[11] and long-term toxicity studies also revealed no changes in histology or markers of inflammation.[8] Moreover, by varying the copolymer structure and molar mass, the size of the nanocarriers can be tuned to allow efficient permeation through different biological barriers,[12] including the leaky vasculature of solid tumors.[1,13,14] Recently, it has been reported that the physicochemical properties of these nanomaterials can be further controlled by designing complex macromolecular architectures (such as comb-like and brush block structures).[15] The topology of PCL-PEG copolymers may represent a key feature for the design of efficient nanocarriers for drug delivery,[16,17] as it may be optimized to enhance nanoparticle self-assembly,[8,18] drug loading,[8,19] as well as polymer functionality.[20] The latter can be further exploited to obtain stimuli-responsive nanomaterials.

Accordingly, specific bioactive moieties, such as stimuli-responsive peptides, can be conjugated to PCL-PEG copolymers, in order to maintain the stealth property during circulation, with the ability to specifically interact with cancer cells upon arrival at the target tumor microenvironment (activable nanocarriers).[8,21] This approach is meant to improve drug therapeutic effectiveness while reducing adverse side effects associated with high dosage and prolonged administration.[22−24]

The altered metabolism of cancer cells profoundly shapes the surrounding microenvironment. Higher glycolysis and plasma membrane proton pump activity in tumor cells cause the excessive production and release of lactic acid in the extracellular milieu, determining a change of the extracellular pH toward acidic values (6.5−7.2).[25,26] Furthermore, the overproduction of enzymes such as matrix metalloproteinases (MMPs), which is also a common trait of tumors, favor the establishment of primary tumors through the remodeling of the extracellular matrix and promote angiogenesis, metastasis, and extracellular signaling events involved in tumor propagation.[27,28]

Metastases of solid tumors generally occur in organs which are distant from the primary tumor lesion.[29−31] Differently, local invasion is a unique characteristic of brain tumor invasion. Indeed, MMP2 levels of expression strongly correlate with high-grade gliomas and glioblastoma (GBM) progression. The release of elevated amounts of MMP2 in the tumor milieu causes the degradation of the extracellular matrix and basement membrane, allowing GBM cells to spread into the brain parenchyma, where the presence of the blood-brain barrier protects them from drug insults.[32]

Activable nanocarriers sensing the unique features of the tumor microenvironment (pH and/or MMP enzymatic activity) elicit localized drug release, leading to increased drug concentration at the tumor site compared to normal tissues.[22,33,34] The use of a low molecular weight protamine peptide (LMWP) coupled to an MMP2/9 activable peptide sequence (ALMWP) was proposed as an innovative strategy to increase tumor targeting efficiency combined to reduced nonselective accumulation in the nontarget cells.[21,35,36] Protamines are short peptides enriched in arginine that confers them high cell penetrating ability and are thus properly considered cell penetrating peptides (CPPs).[37,38] As the nonselective mechanisms of CPP cellular entrance, LMWPs generate important side effects when utilized to deliver drug-loaded nanocarriers.[39,40] The linking of a LMWP to a MMP-sensitive sequence makes LMWP-nanocarriers activable in MMP-rich environments like tumors.[40−42]

In this study, we propose the synthesis of drug-loaded polymer NPs based on PEG-PCL copolymers of complex macromolecular architecture and demonstrated that, by tuning self-assembly and ALMWP sequence conjugation, the uptake and cytotoxicity of the anticancer drug doxorubicin (DOX) are enhanced in MMP2-rich GBM cells while are absent in MMP2-negative cells.

MATERIALS AND METHODS

Materials. Chemicals were purchased from Sigma-Aldrich (Merck) and used without further purification, unless otherwise indicated. The two thiol-containing peptides low molecular weight protamine (LMWP, sequence: CVSRRRRRRGGRRRR) and activable low molecular weight protamine (ALMWP, sequence: EEEEEEEEEEPLGLAGVSRRRRRRGGRRRRC) were purchased from CASLO ApS. When anhydrous and oxygen-free conditions were required, the reactions were performed under nitrogen atmosphere and solvents were degassed prior use for 10 min. Deionized water (18.2MΩ) was obtained from a Millipore Milli-Q purification unit.

Instrumental Setup. ^{1}H NMR experiments were recorded on a Bruker Avance 400 MHz instrument at 298 K, using $CDCl_3$ and DMSO-d_6 as the solvent. Chemical shifts (δ) are reported in ppm downfield from the deuterated solvent as internal standard, and coupling constants (J) are reported in Hz.

For each polymerization, the monomer conversion (χ) was calculated from the ^{1}H NMR spectra of the unpurified samples at the end of the reaction. After ATRP, the integral of the vinyl proton of the unreacted monomer (at δ = 5.7 ppm in $CDCl_3$) was compared with the integral of the protons of the methyl groups along the polymer backbone (δ = 0.7−1.3 ppm). The average degree of polymerization was calculated as DP = $\chi \times M/I$ (where M and I are the moles of monomer and initiator added at the beginning of the polymerization, respectively), and the number-average molar mass was calculated as M_n = DP × M_m (where M_m is the molar mass of the monomer).The number-average molar mass was also calculated by size exclusion chromatography (SEC), together with the dispersity ($Đ$) values, using a Jasco LC-2000Plus chromatograph equipped with a refractive index detector (RI-2031Plus, Jasco) using three Agilent PLC gel columns, 5 μM particle size, 300 × 7.5 mm (MW range: 5 × 10^2−17 × 10^5 g/mol). THF (containing 250 ppm BHT as inhibitor ACS reagent, ≥99.0) was used as the eluent at a flow rate of 1 mL/min at 35 °C. The SEC samples were dissolved in THF at a concentration of 4 mg/mL, filtered through 0.22 μm PTFE syringe filters and injected using a Jasco AS-2055Plus autosampler. The instrument was calibrated using polystyrene standards (by RESTECK and Sigma-Fluka).

Particle size distribution the colloidal nanocarriers in water and aqueous suspensions (PBS 10 mM, pH 7.4) at 25 °C were evaluated via dynamic light scattering (DLS) using a Malvern Instrument Zetasizer Nano ZS equipped with a 4 mW He−Ne laser operating at λ = 634 nm, backscattered angle 173°.

Transmission electron microscopy (TEM) images were acquired with a DeLong America LVEM5 microscope, equipped with a field-emission gun and operating at 5 kV. A volume of 10 μL of nanoparticle suspension in water (10 mg/mL) was dropped on a copper grid (400 mesh) placed on filter paper. The grid was left to dry overnight to evaporate the solvent. TEM image analysis was performed using ImageJ software.

The DOX encapsulation efficiency and DOX release were determined by using a spectrofluorometer (Jasco FP-8500) equipped with a 150 W Xe lamp as the excitation source (λex/λem = 480/587 for DOX dissolved in DMSO, and λex/λem = 480/555 nm for DOX solutions in PBS buffer).

https://doi.org/10.1021/acsapm.2c00897
ACS Appl. Polym. Mater. 2022, 4, 8043−8056

Synthesis of the Copolymers. The PCL-based macromonomer PCLMA (DP_{CL} = 5), the linear copolymer $[PCLMA_4$-*co*-$PEGMA_{16}]_1$, the 4-arm $[PCLMA_4$-*co*-$PEGMA_{16}]_4$, and the macroinitiator $[PCL_{10}$-$Br]_4$ were synthesized as reported in our previous work.[19]

$[PCL_{10}$-*b*-$(PCLMA_4$-*co*-$PEGMA_{16})]_4$ was synthesized as follows. THF (inhibitor free) was degassed under nitrogen for 15 min. A catalyst solution was prepared in a Schlenk tube by adding 100 mg of copper(I)bromide and performing three cycles vacuum-nitrogen. THF (1.2 mL) and 1,1,4,7,10,10-hexamethyltriethylenetetramine (HMTETA) (0.19 mL) were added, and the obtained solution was stirred under nitrogen atmosphere for 10 min at room temperature. $[PCL_{10}$-$Br]_4$ (450 mg, 87 μmol, 1 equiv), poly(ethylene glycol) methyl ether methacrylate (PEG, Mn 500 g·mol^{-1}, 2.8 g, 5.6 mmol, 64 equiv = 16 equiv for each arm) and PCL (1 g, 1.4 mmol, 16 equiv = 4 equiv for each arm) were added in a Schlenk tube (macromonomers concentration = 0.9 M), and three cycles of vacuum-nitrogen were performed. Finally, THF (7.18 mL) and the catalyst solution (0.6 mL, containing CuBr 50.24 mg, 0.35 mmol, 4 equiv, and HMTETA 80.7 mg, 0.35 mmol, 4 equiv) were added to the reaction Schlenk and left under magnetic stirring for 6 h at 50 °C under N_2 atmosphere.

The crude product was then purified by filtration through a neutral alumina pad (h 4 cm, Φ 2 cm) and washing with THF. The filtrate was then dried under reduced pressure, dissolved in 4 mL of dichloromethane (DCM) and dropped in 200 mL of cold hexane. The mixture was stored at −20 °C overnight and subsequently isolated by removing the supernatant. The precipitate was dried under reduced pressure, obtaining 3.98 g of final product. Conversion = 90%; yield = 95%; $\%PEG_{NMR}$ = 79; $M_{n,NMR}$ = 48220 g·mol^{-1}; $M_{n,SEC}$ = 23200 g· mol^{-1}; $Đ$ = 1.20.

^{1}H NMR (400 MHz, Chloroform-d) δ (ppm). δ 4.23 (m, 4H·*x*, PCLMA: −C(O)OC**H$_2$**C**H$_2$**OC(O)-backbone), 4.03 (t, *J* = 6.6 Hz, 2H·*z*+2H·(*n*-1)·*x*+2H·*y*, CL: −C**H$_2$**OC(O)CCH$_3$CH$_3$-backbone, PCLMA: −C**H$_2$**OC(O)−, PEGMA: −CH$_2$C**H$_2$**OC(O)-backbone), 3.62 (t, *J* = 4.9 Hz, 4H·(*m*-1)·*y*, PEGMA: −C**H$_2$**CH$_2$−OC(O)-backbone, −C**H$_2$**C**H$_2$**−), 3.51−3.53 (m, 2H·*y*+2H·*x*, PEGMA: −CH$_2$C**H$_2$**OCH$_3$, PCLMA: −CH$_2$C**H$_2$**OH), 3.35 (s, 3H·*y*,-OC**H$_3$**), 2.28 (t, *J* = 7.5 Hz, 2H·*z*+2H·*n*·*x*, PCLMA: −OC(O)C**H$_2$**CH$_2$), 1.90 (bs, 2H·(*x* + *y*), −C**H$_{2,backbone}$**) 1.66−1.54 (m, 4H·*z*+4H·*n*·*x*, PCLMA: −OC(O)CH$_2$C**H$_2$**−, −C**H$_2$**CH$_2$OC(O)−), 1.40−1.32 (m, 2H·*z*+2H·*n*·*x*, PCLMA: −CH$_2$C**H$_2$**CH$_2$−), 1.15−0.74 (m, 3H·(*x* + *y*), −C**H$_{3,backbone}$**), where *z* is CL degree of polymerization, *n* is PCLMA degree of polymerization, *m* is PEGMA degree of polymerization, *x* is PCLMA repeating units, and *y* is PEGMA repeating units.

Synthesis of $[PCL_{10}$-*b*-$(PCLMA_4$-*co*-$PEGMA_{16})]_4$ Acrylated. $[PCL_{10}$-*b*-$(PCLMA_4$-*co*-$PEGMA_{16})]_4$ (2.21 g, 45.85 μmol, 1 equiv of PCL−OH) was added in a flask which was evacuated and backfilled with N_2 three times. Then 19 mL of anhydrous toluene was added to the dissolved polymer and the flask was cooled down to 0 °C for 20 min. Triethylamine (TEA) (376 μL, 2.697 mmol, 3.6 equiv) and acryloyl chloride (178 μL, 2.191 mmol, 2.9 equiv) were sequentially added to the reaction mixture. The reaction was stirred at room temperature under nitrogen atmosphere overnight. The crude was filtered through a Celite pad (h 4 cm, Φ 2 cm) and washed with toluene. It was then dissolved in 48 mL of DCM and washed with brine (24 mL × 3). The organic phase was dried over sodium sulfate, filtered, and dried under reduced pressure. Precipitation was performed dissolving the polymer in 3.5 mL of DCM and dropped in 130 mL of vigorously stirred cold hexane. After 30 min, the supernatant was removed, and the precipitate was dried under reduced pressure, obtaining 1.35 g of the final product. Conversion = 72%; yield = 70%.

^{1}H NMR (400 MHz, Chloroform-d) δ (ppm). 6.39−6.37 (d, J = 17.3 Hz, 1H·*x*, −CH$_2$OC(O)CHC**H$_2$**), 6.21−5.98 (m, 1H·*x*, −CH$_2$OC(O)C**H**CH$_2$), 5.82 (d, J = 10.4 Hz, 1H·*x*, −CH$_2$OC(O)CHC**H$_2$**), 4.25 (m, 4H·*x*, PCLMA: −C(O)OC**H$_2$**C**H$_2$**OC(O)-backbone), 4.06 (t, *J* = 6.6 Hz, 2H·*z*+2H·*n*·*x*+2H·*y*, CL: −C**H$_2$**OC(O)CCH$_3$CH$_3$-backbone, PCLMA: −C**H$_2$**OC(O)−, PEGMA: −CH$_2$C**H$_2$**OC(O)-backbone), 3.64 (t, *J* = 4.9 Hz, 4H·(*m*-1)·*y*, PEGMA: −C**H$_2$**CH$_2$−OC(O)-backbone, −C**H$_2$**C**H$_2$**−), 3.59−3.46 (m, 2H·*y*+2H·*x*, PEGMA: −CH$_2$C**H$_2$**OCH$_3$, PCLMA: −CH$_2$C**H$_2$**OH), 3.37 (s, 3H·*y*, -OC**H$_3$**), 2.30 (t, *J* = 7.5 Hz, 2H·*z*+2H·*n*·*x*, PCLMA: -OC(O)-C**H$_2$**CH$_2$), 1.93 (bs, 2H·(*x* + *y*), −C**H$_{2,backbone}$**), 1.65 (m, 4H·*z*+4H·*n*·*x*, PCLMA: −OC(O)CH$_2$C**H$_2$**−, −C**H$_2$**CH$_2$OC(O)−), 1.50−1.26 (m, 2H·*z*+2H·*n*·*x*, PCLMA: −CH$_2$C**H$_2$**CH$_2$−), 1.18−0.73 (m, 3H·(*x* + *y*), −C**H$_{3,backbone}$**); where *z* is CL degree of polymerization, *n* is PCLMA degree of polymerization, *m* is PEGMA degree of polymerization, *x* is PCLMA repeating units and *y* is PEGMA repeating units.

Peptide Conjugation through Michael Type Addition. An amount of 19 mg of $[PCL_{10}$-*b*-$(PCLMA_4$-*co*-$PEGMA_{16})]_4$ acrylated was dissolved in 1 mL of acetone and added dropwise into 1 mL of stirred PBS (10 mM pH 7.4). After 5 min, acetone was removed under reduced pressure (under controlled gradient of pressure: from 600 to 100 mbar in 30 min and then 1 h at 100 mbar) at 32 °C, obtaining 1 mL of NP suspension in PBS. The peptides in PBS (0.1 equiv for each acrylate group: 891 μL for LMWP, 1.74 mL for ALMWP, from a 1 mg/mL stock solution) and tris(2-carboxyethyl)-phosphine hydrochloride (TCEP) in PBS (0.5 equiv for each acrylate group; from a 8.9 mg/mL stock solution) were mixed in a vial for 5 min, then added dropwise to the $[PCL_{10}$-*b*-$(PCLMA_4$-*co*-$PEGMA_{16})]_4$ Acrylated suspension. The reaction continued overnight under gentle stirring at room temperature. The suspension was purified by ultrafiltration with Centrifugal Filters (molecular weight cutoff (MWCO) 10 000 g/mol, Amicon) at 1500−2000 relative centrifugal force (rcf) for 10 min, washing with 1 mL of PBS for 4 times at least to obtain 1 mL of suspended NPs.

Nanoparticle Preparation. NPs were prepared according to a nanoprecipitation/solvent (acetone) evaporation method.[12,19] Briefly, 19 mg of copolymer was dissolved in 1 mL of acetone, and the solution was added dropwise into 1 mL of PBS (PBS 10 mM pH 7.4) and stirred for 5 min. Acetone was removed at the rotary evaporator under controlled gradient of pressure (from 600 mbar to 100 mbar in 30 min and then 1 h at 100 mbar) at 32 °C. The final suspensions were characterized by Dynamic Light Scattering at 25 °C to evaluate their size distribution.

DOX Loading. Nineteen mg of copolymer were dissolved in 1 mL of acetone containing 1.5 mg of doxorubicin hydrochloride (DOX-HCl) in the presence of 0.71 μL of triethylamine (TEA). The solution was added dropwise into 1 mL of PBS and stirred for 5 min.

In the case of DOX encapsulation in peptide-conjugated copolymers, 1.5 mg of DOX-HCl was dissolved in 1 mL of acetone with 0.71 μL of TEA, and this solution was then added dropwise to the polymer suspension in PBS (19 mg/mL) and stirred for 10 min.

Acetone was removed with the rotary evaporator under a controlled gradient of pressure (from 600 to 100 mbar in 30 min and then 1 h at 100 mbar) at 32 °C. The unloaded DOX was removed by ultrafiltration with Centrifugal Filters (MWCO 10 000 g/mol, Amicon) at 1500−2000 rcf for 10 min, washing with 1 mL of PBS four times to obtain 1 mL of DOX-loaded NPs.

The encapsulation of DOX was evaluated by spectrofluorometry using a Jasco FP-8500. An amount of 20 μL of the NP suspension was withdrawn, dried under compressed air overnight, and dissolved in 1 mL of DMSO in the presence of 0.71 μL of TEA. The fluorescence intensity was measured by using the spectrofluorimeter at a λ_{ex} = 480 nm and a λ_{em} = 587 nm. The amount of DOX encapsulated in the NPs was assessed with the use of a calibration curve that correlated the measured intensity to the amount of DOX in DMSO. Drug loading (DL) and encapsulation efficiency (EE) were calculated according to the following equations:

$$\text{DL [\%]} = \frac{\text{encapsulated drug [mg]}}{\text{encapsulated drug [mg]} + \text{polymer [mg]}} \times 100$$

$$\text{EE [\%]} = \frac{\text{encapsulated drug[mg]}}{\text{feed drug [mg]}} \times 100$$

DOX Release. DOX release studies from peptide-conjugated NPs were performed in PBS (10 mM, pH = 7.4) at 37 °C. Briefly, a PBS

https://doi.org/10.1021/acsapm.2c00897
ACS Appl. Polym. Mater. 2022, 4, 8043−8056

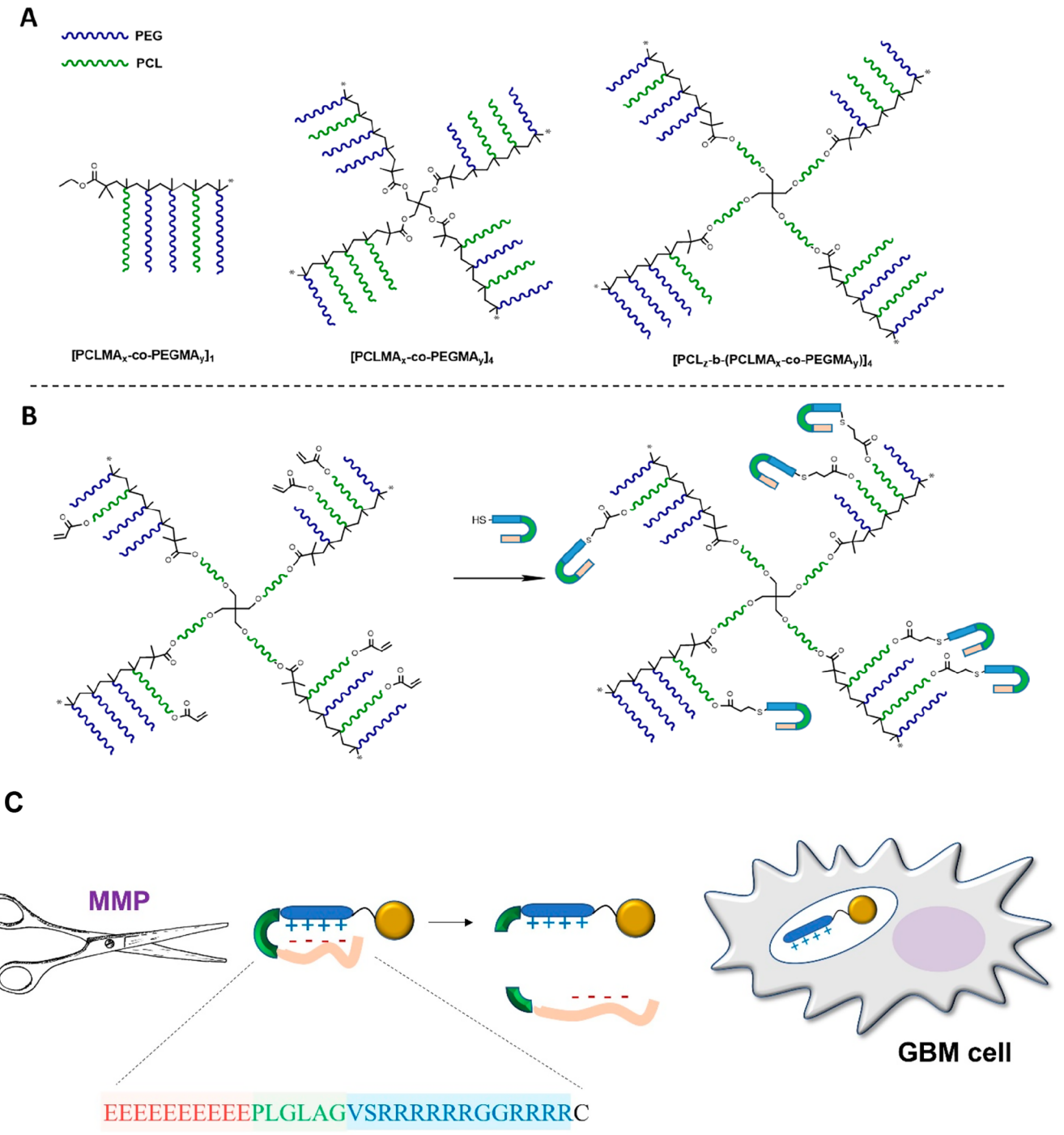

Figure 1. (A) Schematic representation of the linear and 4-arm PEG-PCL copolymers. (B) After acrylation of PCL side chains, the peptides can be conjugated by Michael type addition. (C) ALMWP peptide includes a polyanionic domain (pink), polycationic LMWP sequence (blue), and MMP cleavable sequence (green).

solution of NPs was diluted to obtain a final concentration of polymer of 2 mg/mL and 2 mL of the sample was dialyzed against 100 mL of PBS buffer (10 mM, pH 7.4) at 37 °C (regenerated cellulose dialysis membrane, 6000−8000 g/mol cutoff). At selected times, small aliquots (1 mL) of release medium were withdrawn and replaced with an equal volume of PBS. The samples were analyzed by using a spectrofluorimeter (Jasco FP-8500) at λex/λem = 480/555 nm. The amount of released DOX was quantified using the standard curve prepared for DOX in PBS. The standard curve was obtained by measuring the fluorescence intensity (λex/λem = 480/555 nm) of different concentrations of DOX solution in PBS. The percentage of released DOX at each time point was calculated according to the following equation:

$$\text{drug release}|_{t=i}(\%) = \frac{\mu g_{\text{DOXO}}|_{t=i}^{\text{bath}} + \sum_{t=0}^{i-1} \mu g_{\text{DOXO}}|^{\text{sample}}}{\mu g_{\text{DOXO}}|_{\text{end}}^{\text{bath}} + \sum_{t=0}^{\text{end}-1} \mu g_{\text{DOXO}}|^{\text{sample}}}\%$$

where μg_{DOXO} is the DOX amount contained in the bath (100 mL) and in each sample (1 mL) at different time points.

Cell Line Establishment and Culture. ICH001, ICH003, and ICH013 cell lines were obtained from GBM surgical samples of

https://doi.org/10.1021/acsapm.2c00897
ACS Appl. Polym. Mater. 2022, 4, 8043−8056

patients undergoing surgery for brain tumor removal. Surgical specimens were collected from consenting patients at the Neurosurgery Department, Humanitas Research Hospital (Rozzano, Italy) under "Humanitas" research ethics committee approval. Tumor samples were processed as outlined by Gritti et al.[43] Briefly, tumor tissues were quickly dissected with scalpels and incubated (20 min at 37 °C) with collagenase (Thermo Fisher, Waltham, MA, USA) and DNase-I (Sigma-Aldrich, St. Louis, MO, USA) to obtain a single cell suspension. After hypotonic shock to eliminate erythrocytes, the cell suspension was filtered through a 40 μm strainer and cells were incubated in Neurocult medium supplemented with hormone mix, and heparine (STEMCELL Technologies, Vancouver, Canada) supplemented with FGF (20 ng/mL) and EGF (20 ng/mL) (Peprotech, Cranbury, NJ, USA). Brain tumor-derived neurospheres were evident as early as 1 week after plating. Spheres were grown for at least 3 weeks until they reached an adequate size for plating and passaging (~200 μm). Human endothelial cells (hCMEC/d3) were purchased from Millipore (Temecula, CA, USA) and cultured in Endothelial Cell Growth Basal Medium-2 (Lonza, Basel, Switzerland) supplemented with FGF (20 ng/mL) (Peprotech) according to manufacturing instructions.

Live and Confocal Imaging Microscopy. GBM cells (5×10^3/well) were seeded in a 96-well "flat bottom" precoated (5 μg/mL collagen, 1 μg/mL fibronectin) plate. Cells were incubated (5 h) with DOX-loaded nanocarriers at a fixed DOX concentration of 1.2 μg/mL. Nuclear DOX accumulation was monitored once per hour by DMi8 fluorescent microscopy and LasX software (Leica Microsystems GmbH). The DAPI (ex/em: 405/415−450 nm) and DOX autofluorescence (488/570−700) signals were acquired sequentially at 20× magnification. Images were processed using ImageJ (Wayne Rasband, National Institute of Mental Health, Bethesda, MD, USA) using the DAPI signal to determine the nucleus area. The DOX fluorescence was quantified as mean gray values in the nucleus area.

hCMEC/D3 cells were seeded on glass coverslip at concentration of 3500 cell/cm^2. After 24 h, cells were incubated with DOX-loaded nanocarriers ([DOX] 1.2 μg/mL) for 5 h in complete medium. Cells were then fixed in PFA 4% for 15 min and incubated (1 h) with anti-Phalloidin conjugated with Alexa Fluor 647 (1:200, Thermo Fisher, Waltham, Mas). Images of the cells in different experimental conditions were acquired by means of a SP8II confocal microscope and LasX software (Leica Microsystems GmbH) with the HCX PL APO 63×/1.4 oil objective. The DAPI (ex/em: 405/415−450 nm), Phalloidin-Alexa Fluor 647 (ex/em: 650/665 nm) and DOX autofluorescence (488/570−700) signals were acquired sequentially at a high scan rate. Images were processed using ImageJ (Wayne Rasband, National Institute of Mental Health, Bethesda, MD, USA) using the DAPI signal to segment the nucleus and the Phalloidin signal to identify the cell contour. The DOX fluorescence was quantified in the nuclei as mean gray values in the optical section where the nucleus area was maximized

MMP2 Enzymatic Activity. MMP2 enzymatic activity was determined by zymography as described in the literature.[44] Briefly, 5 μL of cell conditioned medium was loaded in an 8% polyacrylamide gel supplemented with 0.1% gelatin B (MMP2 substrate). After running at 90 V voltage for 2 h, the gel was washed three times with Zymogram Renaturation Buffer, incubated with Zymogram Development Buffer (BioRad, Hercules, CA) for about 12 h at 37 °C, and finally incubated with Safe Comassie (BioRad, Hercules, CA) for 2 h and destained in dH_2O until the desired blue coloring. The digestion intensity was determined by ChemiDoc Imaging System (BioRad, Hercules, CA) and analyzed by Image Lab software (BioRad).

***In Vitro* Viability Assay.** GBM cells (10^4 cells/well) or endothelial hCMEC/D3 cells (5×10^3 cells/well) were plated in 96-well plates in a final volume of 200 μL of medium in the absence/presence of increasing doses of different NPs, at the indicated doses of DOX. The mitochondrial enzymatic activity, an indicator of cell viability, was assessed by MTT assay. Briefly, 4 h before the end of the treatment, 3-[4,5-dimethylthiazole-2-yl]-2,5-diphenyltetrazolium bromide (MTT) was added to a final concentration of 0.5 mg/mL. At the end of the treatment, the plate was centrifuged at 1500 rpm for 15 min to pellet down the cells. The supernatant was removed, and 100 μL of DMSO was added to each well to solubilize the formazan salt crystals. After 15 min of shaking at room temperature, absorbance was read at 570 and 630 nm. The final absorbance values were determined by subtracting the value recorded at 630 nm from that measured at 570 nm.

RESULTS AND DISCUSSION

PCL-PEG copolymers with complex topologies were synthesized through controlled polymerization techniques such as ring opening polymerization (ROP) and atom transfer radical polymerization (ATRP)[19] in order to achieve a predetermined degree of polymerization (DP) and low dispersity ($Đ$). While ROP was used to synthesize the PCL-based macromonomer and a 4-arm macroinitiator, ATRP was used to copolymerize the PEG-based macromonomer and to obtain linear, 4-arm comb-like copolymers and brush block copolymers (Figure 1A). Polymer design included the acrylation of the terminal hydroxyl groups of the PCL side chains, to achieve a facile peptide conjugation via Michael type addition[45] (Figure 1B), by using either the activable peptide sequence ALMWP (Figure 1C) or the low molecular weight protamine peptide (LMWP) as control.

Polymers Synthesis and Characterization. The PCL-based macromonomer (PCLMA, 5 CL repeating units (DP = 5)) was first synthesized through a bulk ROP of the ε-caprolactone (ε-CL) with tin(II) 2-ethylhexanoate as the catalyst and hydroxyethyl methacrylate (HEMA) as the initiator.[19,45]

The linear copolymers $[PCLMA_x\text{-}co\text{-}PEGMA_y]_1$ were synthesized through ATRP by random copolymerization of commercially available poly(ethylene glycol)methyl ether methacrylate (PEGMA, average M_n = 500 g/mol, with 8/9 ethylene oxide repeating units) and PCLMA in the presence of Cu(I)Br/1,1,4,7,10,10-hexamethyltriethylenetetramine (HMTETA) catalyst, and ethyl α-bromoisobutyrate as initiator, as previously reported.[12,19] Similarly, the 4-arm copolymers $[PCLMA_x\text{-}co\text{-}PEGMA_y]_4$ were obtained using the same ATRP procedure but with pentaerythritol tetrakis(2-bromoisobutyrate) as multifunctional initiator.[19]

A 4-arm PCL-based ATRP macroinitiator (z = 10 is the number of CL repeating units per arm) was also synthesized as described in our previous work.[12,19] The ATRP of the PCLMA and PEGMA mixture was finally carried out from this macroinitiator to obtain the 4-arm comb-like structure $[PCL_z\text{-}b\text{-}(PCLMA_x\text{-}co\text{-}PEGMA_y)]_4$. This macromolecular architecture was designed to include an additional PCL star core, which was expected to provide further hydrophobic interactions for self-assembly and drug loading.

Regarding the PCLMA-PEGMA copolymerization, a DP value of 20 and a PEG/PCL molar ratio of 8:2 were targeted (x = 4 and y = 16 for all the linear and the 4-arm architectures), in order to promote the self-assembly and formation of small and stable NPs, as evaluated in our previous work,[12,19,20] while obtaining a sufficient number of hydroxyl groups (i.e., the terminal group of each PCLMA repeating unit) for further functionalization.

All the polymerizations achieved high conversions (≥84% after 6 h), as calculated from ^{1}H NMR spectroscopy.

Similar to the cases of $[PCLMA_4\text{-}co\text{-}PEGMA_{16}]_1$ and $[PCLMA_4\text{-}co\text{-}PEGMA_{16}]_4$, the semilogarithmic kinetic plot of $[PCL_{10}\text{-}b\text{-}(PCLMA_4\text{-}co\text{-}PEGMA_{16})]_4$ also revealed a first order kinetics (Figure S1, Supporting Information), demonstrating a

https://doi.org/10.1021/acsapm.2c00897
ACS Appl. Polym. Mater. 2022, 4, 8043−8056

Table 1. Summary of Properties of the Copolymers[a]

name	EO/CL[mol:mol]	X_{CL} (%)	X_{PCLMA} (%)	X_{PEGMA} (%)	M_{th}(g/mol)	$M_{n,NMR}$(g/mol)	$M_{n,SEC}$(g/mol)	$Đ$
$[PCLMA_4\text{-}co\text{-}PEGMA_{16}]_1$	7.2	99	99	99	10 995	9560	8100	1.16
$[PCLMA_4\text{-}co\text{-}PEGMA_{16}]_4$	7.2	99	84	84	43 932	40 430	17 700	1.12
$[PCL_{10}\text{-}b\text{-}(PCLMA_4\text{-}co\text{-}PEGMA_{16})]_4$	4.8	100	90	90	49 088	48 220	23 200	1.20

[a]Molar ratio between ethylene oxide and ε-caprolactone repeating units (EO/CL), conversion of ε-CL by ROP (X_{CL}), conversion of PCLMA and PEGMA macromonomers (X_{PCLMA} and X_{PEGMA}), theoretical molar mass (M_{th}), number-average molar mass ($M_{n,NMR}$) obtained by ^{1}H NMR ($CDCl_3$), and SEC ($M_{n,SEC}$) respectively, and dispersity $Đ$ (by SEC) are listed in the table (in SEC, THF was the mobile phase and polystyrene standards were used for calibration).

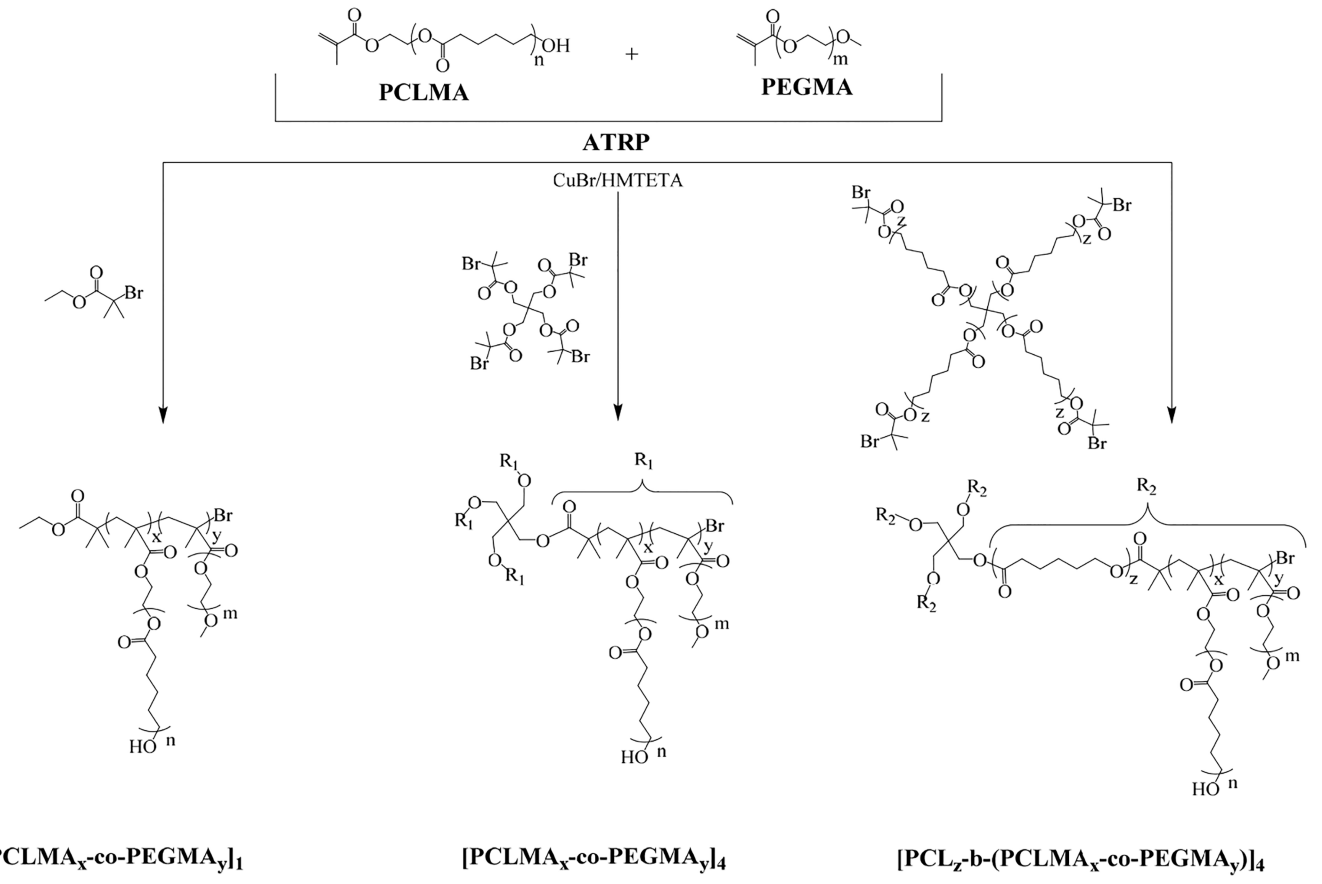

Figure 2. Reaction pathway and nomenclature of the macromolecular structures.

good reaction control over the polymer molar mass and the molar mass distribution, which was also confirmed by the relatively low dispersity $Đ$ obtained from SEC chromatograms (Table 1). The deviation of the number-average molar mass calculated by NMR from the value obtained by SEC was likely to be caused by the intrinsic limitation of SEC to determine the exact molar mass of comb-like and brush block copolymers, as observed in earlier publications.[19,20]

^{1}H NMR was used to characterize each step of the polymer syntheses, and NMR analysis of the purified polymers confirmed the successful copolymerization of PCL blocks and PEGMA for different architectures (Figure 2).

Afterward, acrylation was necessary to make the selected copolymers suitable for a simple and versatile conjugation of the thiolated peptides via Michael type addition.[45] The esterification of the terminal hydroxyl groups of the PCL side chains was carried out in the presence of acryloyl chloride and triethylamine as the base.[45,46] ^{1}H NMR analysis was used to estimate the high conversion of hydroxyl groups to acrylates (70%), as calculated from the integration of the acrylate proton peaks (δ = 5.9−6.4 ppm, Figure 3).

Afterward, $[PCL_{10}\text{-}b\text{-}(PCLMA_4\text{-}co\text{-}PEGMA_{16})]_4$ acrylated was conjugated with the peptides LMWP, ALMWP through a Michael type addition, which was carried out under physiological pH (in PBS, pH = 7.4) at room temperature, in the presence of Tris(2-carboxyethyl) phosphine (TCEP) to prevent disulfide formation.[23,27] A peptide/acrylate molar ratio 1:10 was used to conjugate approximately one peptide to each polymer chain. In this way, we intended to achieve the bioactivity of the macromolecules while maintaining their stealth character. ^{1}H NMR spectra of the conjugated copolymers confirmed the conversion of acrylates into the grafted peptidic moiety (partial disappearance of acrylate peaks at 5.9−6.4 ppm after conjugation, Figure S2, Supporting Information).

Nanoparticle Preparation and Characterization. NPs were prepared according to nanoprecipitation/solvent (acetone) evaporation method.[12,19] Polymers dispersed in

https://doi.org/10.1021/acsapm.2c00897
ACS Appl. Polym. Mater. 2022, 4, 8043−8056

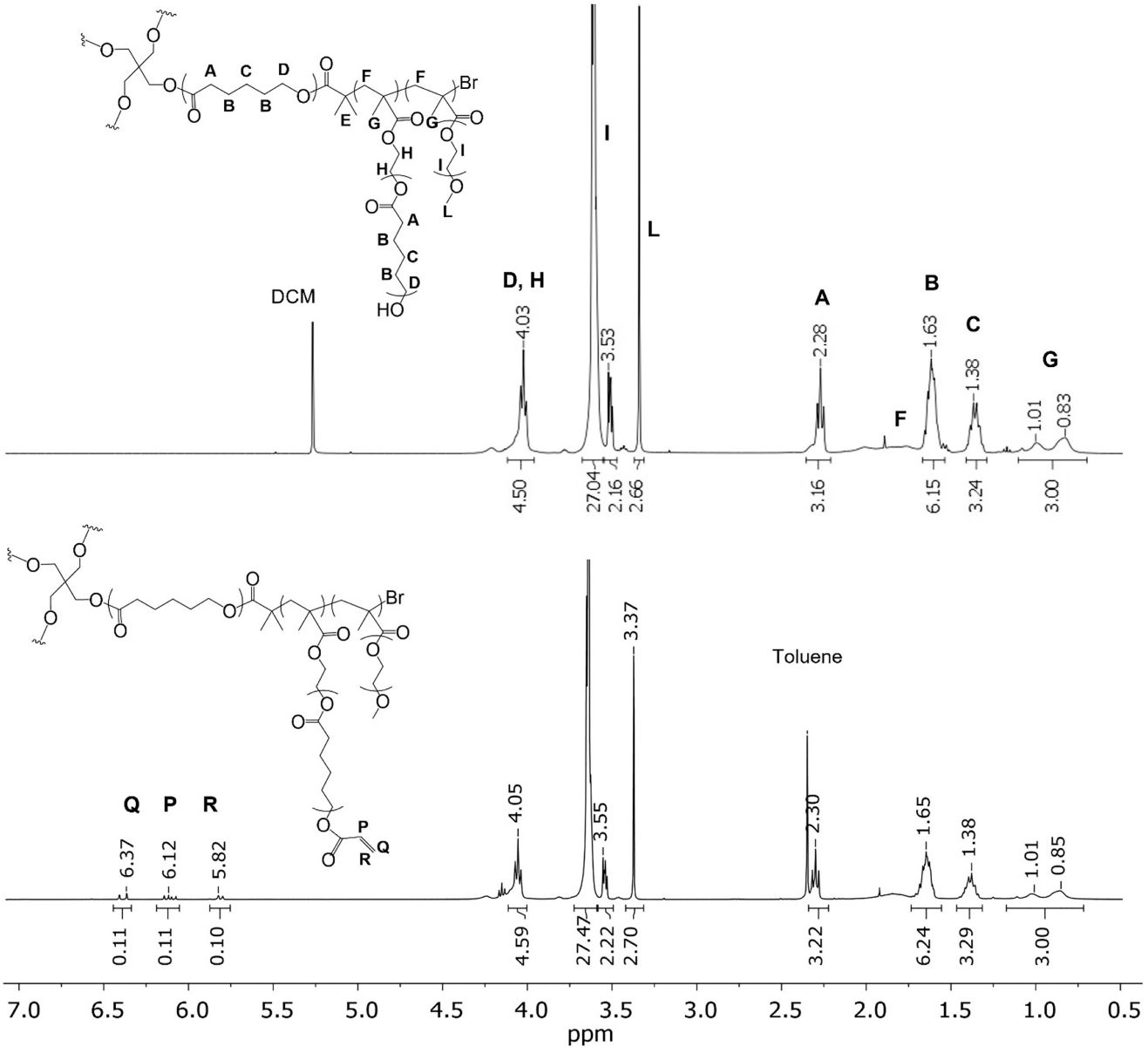

Figure 3. ^{1}H NMR spectra (in $CDCl_3$) of $[PCL_{10}$-*b*-$(PCLMA_4$-*co*-$PEGMA_6)]_4$ before and after acrylation.

physiological buffer (PBS 10 mM pH 7.4) were characterized by DLS analysis. The effect of polymer architecture on particle size is reported in Figure 4. The self-assembled NPs generally presented a bimodal size distribution curve, with the main peak at 6−18 nm and a second one at >100 nm (Figure 4A and B). We compared the characteristic values of the two peaks, i.e., mean size and percent scattering intensity (*I*%), in order to obtain a qualitative comparison of the different nanoparticle populations.[19,20] The smallest peak represented more than 40% of the scattering intensity (Figure 4B), which corresponds to the largest number of particle size of the distribution and is compatible with the size of unimolecular micelles.[19] The formation of larger particles was in agreement with previous works,[19] and it may be due to different kinetic mechanisms of self-assembly related to the preparative method, which may also include the effect of the molar mass dispersity.[19,47−49] The four arm $[PCLMA_4$-*co*-$PEGMA_{16}]_4$ showed a slightly higher average size than the linear $[PCLMA_4$-*co*-$PEGMA_{16}]_1$ and almost a monomodal distribution, which may be due to different kinetic mechanisms of self-assembly related to its multiarm architecture,[19] even though this characteristic was lost when DOX was also loaded (see paragraph below).

Since larger particles provide higher percent of scattering intensity in DLS analysis,[20] we expected that their number was relatively low in these NP suspensions. The predominance of small nanoparticles was confirmed by transmission electron microscopy (TEM) imaging (Figure 4E), where dehydrated $[PCL_{10}$-*b*-$(PCLMA_4$-*co*-$PEGMA_{16})]_4$ nanoparticles of small size (16−32 nm) are shown. Few larger particles (>100 nm) are visible in the TEM images of $[PCLMA4$-*co*-$PEGMA16]_1$, Figure S3, Supporting Information.

As expected, the highest particle size was obtained with $[PCL_{10}$-*b*-$(PCLMA_4$-*co*-$PEGMA_{16})]_4$, which may be ascribed to a larger hydrophobic domain due to the inner PCL star block.

https://doi.org/10.1021/acsapm.2c00897
ACS Appl. Polym. Mater. 2022, 4, 8043−8056

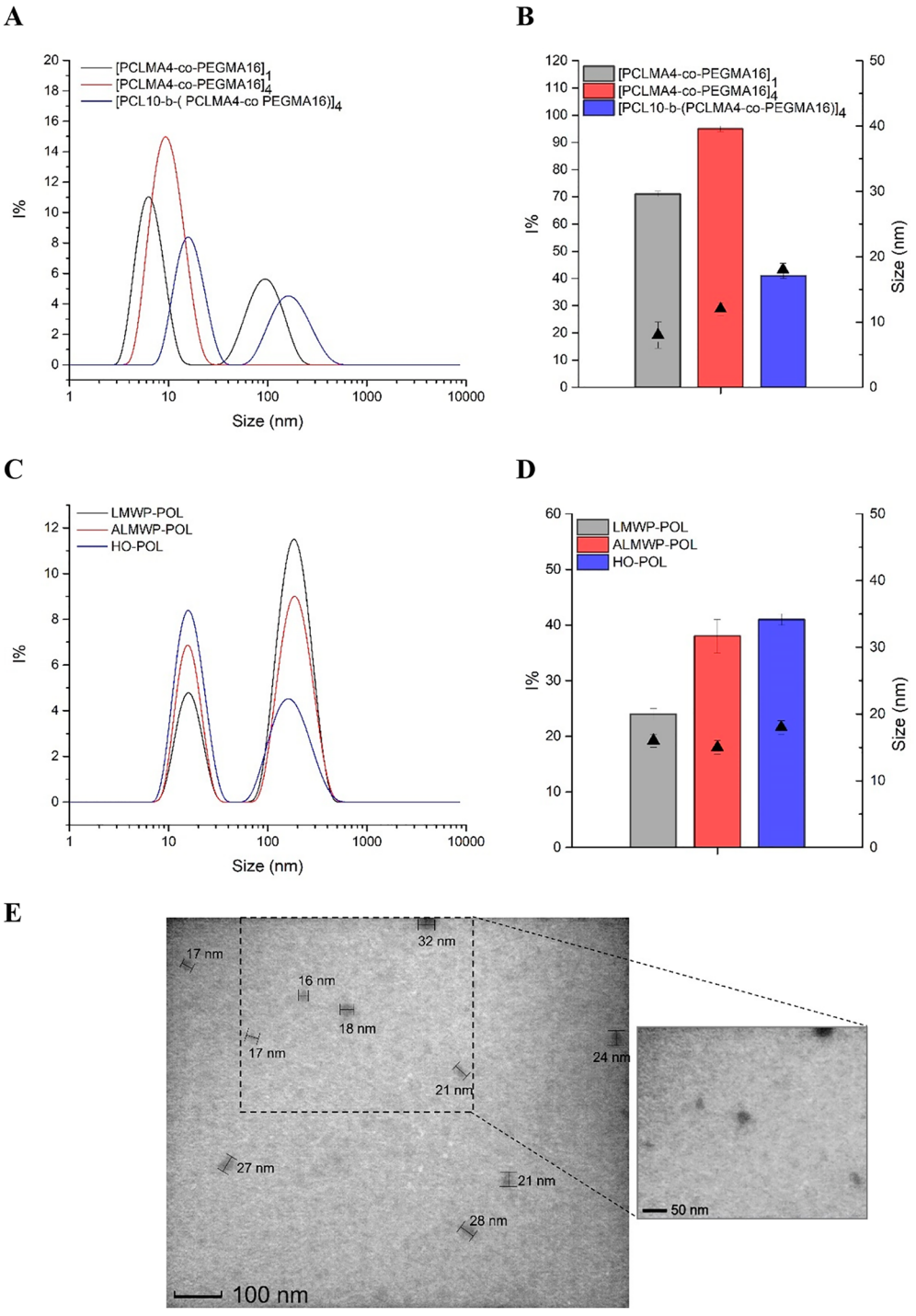

Figure 4. DLS size distribution curves of $[PCLMA_4\text{-}co\text{-}PEGMA_{16}]_1$, $[PCLMA_4\text{-}co\text{-}PEGMA_{16}]_4$, polymers (A) and $[PCL_{10}\text{-}b\text{-}(PCLMA_4\text{-}co\text{-}PEGMA_{16})]_4$ obtained at 25 °C in PBS 10 mM (pH = 7.4, polymer conc. 1 mg/mL). (B) Average size (triangle) and mean scattering intensity percentage (*I*%) (bar) of the inner peak in the size distribution curve of the three polymers. (C) DLS curves of the peptide-conjugated polymers (LMWP-POL, ALMWP-POL) and HO-POL ($[PCL_{10}\text{-}b\text{-}(PCLMA_4\text{-}co\text{-}PEGMA_{16})]_4$). (D) Average size (triangle) and *I*% (bar) of the inner peak of the peptide-conjugated polymers. (E) TEM images of $[PCL_{10}\text{-}b\text{-}(PCLMA_4\text{-}co\text{-}PEGMA_{16})]_4$ nanoparticles; particle size varies within a diameter range of 16−32 nm.

Peptide conjugation seemed not to affect particle size extensively, as evaluated by DLS (Figure 4C and D) and TEM (Figure S3, Supporting Information). When $[PCL_{10}\text{-}b\text{-}(PCLMA_4\text{-}co\text{-}PEGMA_{16})]_4$ was functionalized with the peptides (LMWP-POL, ALMWP-POL), the resulting size distribution curves showed a similar small peak with an average hydrodynamic diameter of ∼16 nm and percent of the scattering intensity (*I*%) up to 38% in the case of ALMWP-POL (Figure 4D). Particle size measured at different temperatures (from 10 to 37 °C) did not show statistically significant variations (Table S1, Supporting Information), thus indicating the absence of a temperature-dependent polymer association (i.e., a lower critical solubility temperature (LCST)

https://doi.org/10.1021/acsapm.2c00897
ACS Appl. Polym. Mater. 2022, 4, 8043−8056

induced by the PEG side chains[50,51]) under physiological temperature conditions.

DOX Loading and Release. DOX was chosen to be encapsulated in the above nanocarriers. DOX is one of the first line chemotherapeutic drugs for a wide range of cancers including carcinomas, sarcomas and hematological cancers.[1,13] Despite its extensive clinical utilization, the nanoencapsulation of this anthracycline is required mainly because of its prominent cardiac toxicity, short half-life and low solubility in aqueous solution, which can hinder its therapeutic potential.[13] In addition, the multidrug resistance of tumor cells, which is attributed to the P-glycoprotein efflux pump on plasma membrane, represents an additional barrier that nanocarriers may overcome for achieving efficient DOX delivery and efficacy.[52]

DOX was encapsulated in the PCL-PEG copolymers via nanoprecipitation/solvent evaporation, dissolving the drug (neutralized by triethylamine) in the acetone phase with the polymer before the formation of the water suspension. The encapsulation efficiency (EE) and drug loading (DL) were determined by fluorimetric analysis, and these values are reported on Table 2, together with particle size as measured after the process.

Table 2. Properties of the DOX-Loaded NPs Obtained by Nanoprecipitation of the Different Polymers[a]

polymer	DL (%)	EE (%)	d_h [nm]	I%
$[PCLMA_4$-*co*-$PEGMA_{16}]_1$	0.7 ± 0.2	9 ± 2	6 ± 1	20 ± 6
$[PCLMA_4$-*co*-$PEGMA_{16}]_4$	0.9 ± 0.2	11 ± 3	9 ± 1	20 ± 9
$[PCL_{10}$-*b*-$(PCLMA_4$-*co* $PEGMA_{16})]_4$	1.0 ± 0.1	13 ± 1	12 ± 1	43 ± 9
LMWP-POL	1.1 ± 0.2	15 ± 2	15 ± 1	22 ± 2
ALMWP-POL	1.3 ± 0.5	16 ± 6	10 ± 1	10 ± 1

[a]Drug loading (DL) and encapsulation efficiency (EE), average hydrodynamic diameter (d_h), mean scattering intensity percentage of the main peak in the size distribution curve (I%) at 25°C in water. EE %, DL%, and d_h indicate the average (±SD) of experiments run in triplicate.

The three copolymers showed similar drug loading (DL% from 0.7 to 1), although $[PCL_{10}$-*b*-$(PCLMA_4$-*co*-$PEGMA_{16})]_4$ presented a slightly higher encapsulation efficiency (13%), which is likely due to the presence of the hydrophobic PCL star block. $[PCLMA_4$-*co*-$PEGMA_{16}]_1$ and $[PCLMA_4$-*co*-$PEGMA_{16}]_4$ tend to aggregate, as suggested by the lower I% of the main size distribution peak when compared with the unloaded NPs (Figure 4D). On the other hand, $[PCL_{10}$-*b*-$(PCLMA_4$-*co*-$PEGMA_{16})]_4$ showed more stability, with size and I% which are similar of the unloaded copolymer. The conjugation of the peptides with this copolymer slightly enhanced the drug loading, and the highest DL and EE were obtained with ALMWP (1.3% and 16%, respectively). In terms of particle stability, the final DOX-loaded NPs conjugated with the peptides presented a similar hydrodynamic diameter to that of the unloaded polymers, although I% was lower, particularly for ALMWP-POL, indicating possible particle aggregation during the encapsulation process.

Finally, drug release tests were carried out under sink conditions in phosphate-buffered saline (PBS 10 mM, pH 7.4) at 37 °C. Release profiles were followed by spectrofluorometry and are shown in Figure 5.

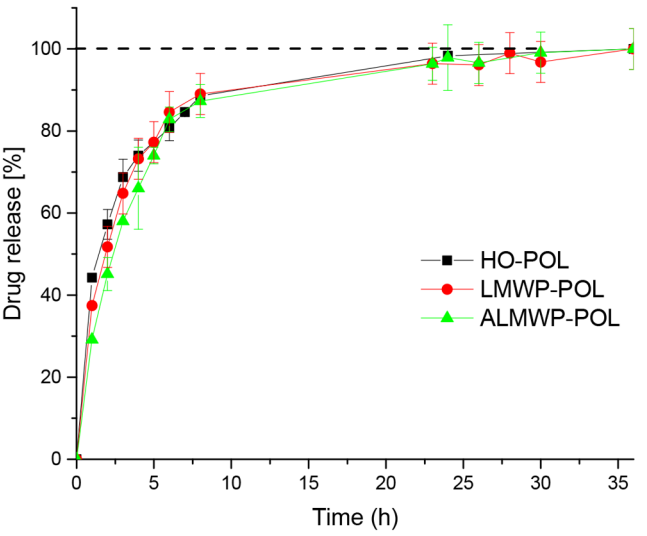

Figure 5. DOX release from polymer OH-POL ($[PCL_{10}$-*b*-$(PCLMA_4$-*co*-$PEGMA_6)]_4$), LMWP-POL, and ALMWP-POL in PBS 10 mM, pH 7.4, at 37 °C. Error bars indicate ± SD from experiments run in triplicate.

DOX release from the two peptide-conjugated NPs did not show very significant variations within the experimental reproducibility of the measurements, and all the percent release curves reached their 100% plateau in almost 24 h. The drug release mechanism was supposed to be purely diffusive, since polymer degradation is negligible within the time scale of the experiment.[53] By applying the Higuchi model in the early stage of release (see the Supporting Information, Figure S4), a typical Fickian diffusion mechanism was confirmed. Thus, diffusion should be controlled by the size of the particles (surface areas) which were all similar for different polymers after DOX encapsulation. The results indicate that the NPs were able to delay the release of the drug if compared to free DOX delivery under sink conditions.[1] The fast release within the first hours of incubation (more than 70% in less than 5 h) may be ascribed to the amphiphilic nature of DOX, which may accumulate at the interface between the hydrophilic and hydrophobic polymer blocks and diffuse rapidly in the water phase.[54]

MMP-Dependent Intracellular Uptake of ALMWP Nanovectors. To verify the efficiency of the MMP-activable functionalization in a MMP-high cellular environment, real-time cellular uptake and internalization of DOX-loaded ALMWP-POL nanovectors were evaluated by live cell microscopy in patient-derived GBM cell lines (ICH001, ICH003, and ICH013) established from tumor resections. All the GBM-derived cell lines were assayed for the expression of the MMP2 enzyme (Figure S5, Supporting Information.). CPP-functionalized nanovectors (LMWP-POL-DOX) and nanovectors without any external decoration (POL-DOX) were included as positive and negative control, respectively.

Nuclear DOX quantification showed a time dependent and significantly higher nuclear DOX accumulation upon cell incubation with ALMWP-POL-DOX (MMP2 activable) and LMWP-POL-DOX compared to nonfunctionalized (POL-DOX) nanovectors (Figure 6 A and B). Noteworthy, the highest and significant DOX accumulation was observed in cells incubated with MMP-activable nanovectors (ALMWP-POL-DOX) (Figure 6A and B).

https://doi.org/10.1021/acsapm.2c00897
ACS Appl. Polym. Mater. 2022, 4, 8043−8056

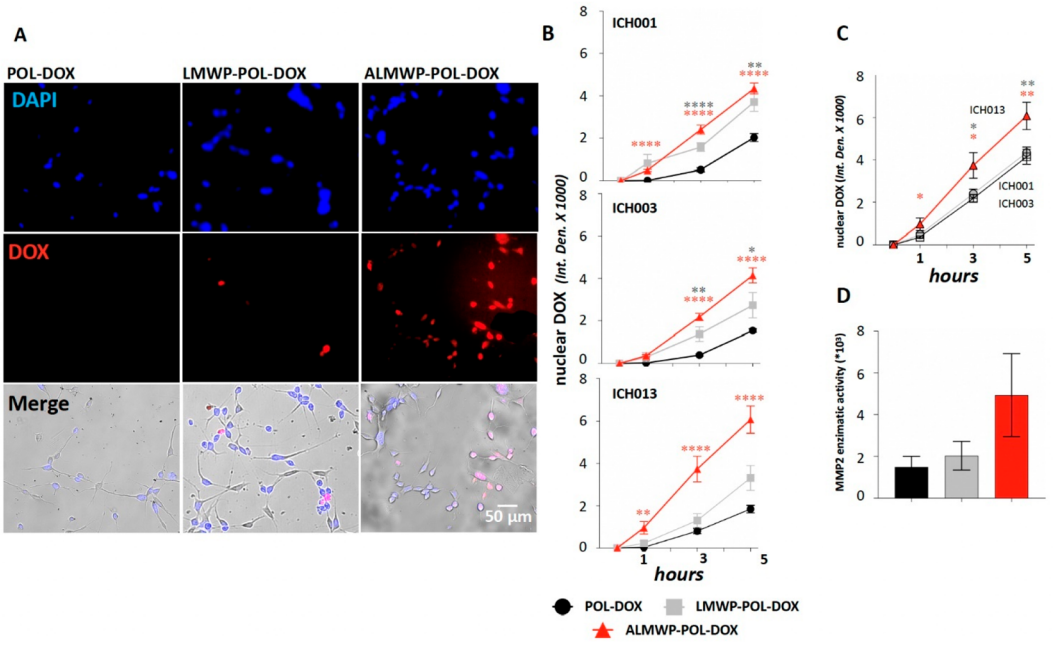

Figure 6. Live imaging uptake. GBM cells were plated and treated with nanovectors at a [DOX] of 1.2 μg/mL. One image per hour was captured for each well with a DMi8 microscope (Leica). (A) Representative live microscopy images of ICH013 cells incubated with the indicated nanovectors for 5h showing DOX (in red) inside the nuclei. DAPI was used for nuclear staining. The lower panel shows bright-field differential interference contrast merged signals. (B) Real-time nuclear DOX quantification expressed as integrated density (Int. Den) ± SE in GBM cells incubated with the indicated POL-DOX nanovectors. Images were analyzed by LAS-X software (Leica). Nuclear DOX amount was quantified in 90−100 cells/time point. (C) Comparison of ALMWP-POL-DOX uptake in ICH001 (black), ICH003 (gray), and ICH013 (red) cells. (D) MMP2 enzymatic activity detected in 24 h cell culture supernatant and assayed by zymography. Values are expressed as the mean ± SE of three independent experiments. Pairwise comparison was performed by Student's t test. *P < 0.05, **P < 0.01, ****P < 0.0001.

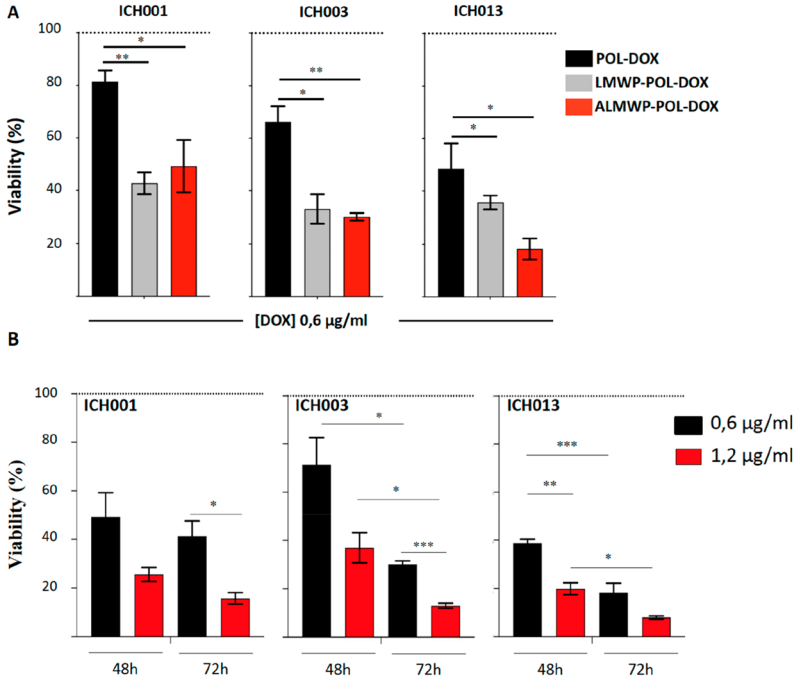

Figure 7. Viability assay. (A) Cell viability assayed by MTT test on ICH001, ICH003, and ICH013 cells after 48 h of incubation with the indicated nanovectors at [DOX] of 0.6 μg/mL. (B) Cell viability assayed by MTT test after 48 and 72 h incubation with ALMWP-POL-DOX at [DOX] of 0.6 or 1.2 μg/mL. Values are expressed as mean percentage survival of four replicates ± SE normalized to corresponding untreated cells cultured without nanovectors. Pairwise comparison was performed by Student's t test. *P < 0.05,**P < 0.01, ***P < 0.001.

A different nuclear DOX accumulation was observed after ALMWP-POL-DOX incubation. Consistent with a higher MMP2 enzymatic activity, a significant higher DOX accumulation was observed in ICH013 compared to ICH001 and

https://doi.org/10.1021/acsapm.2c00897
ACS Appl. Polym. Mater. 2022, 4, 8043−8056

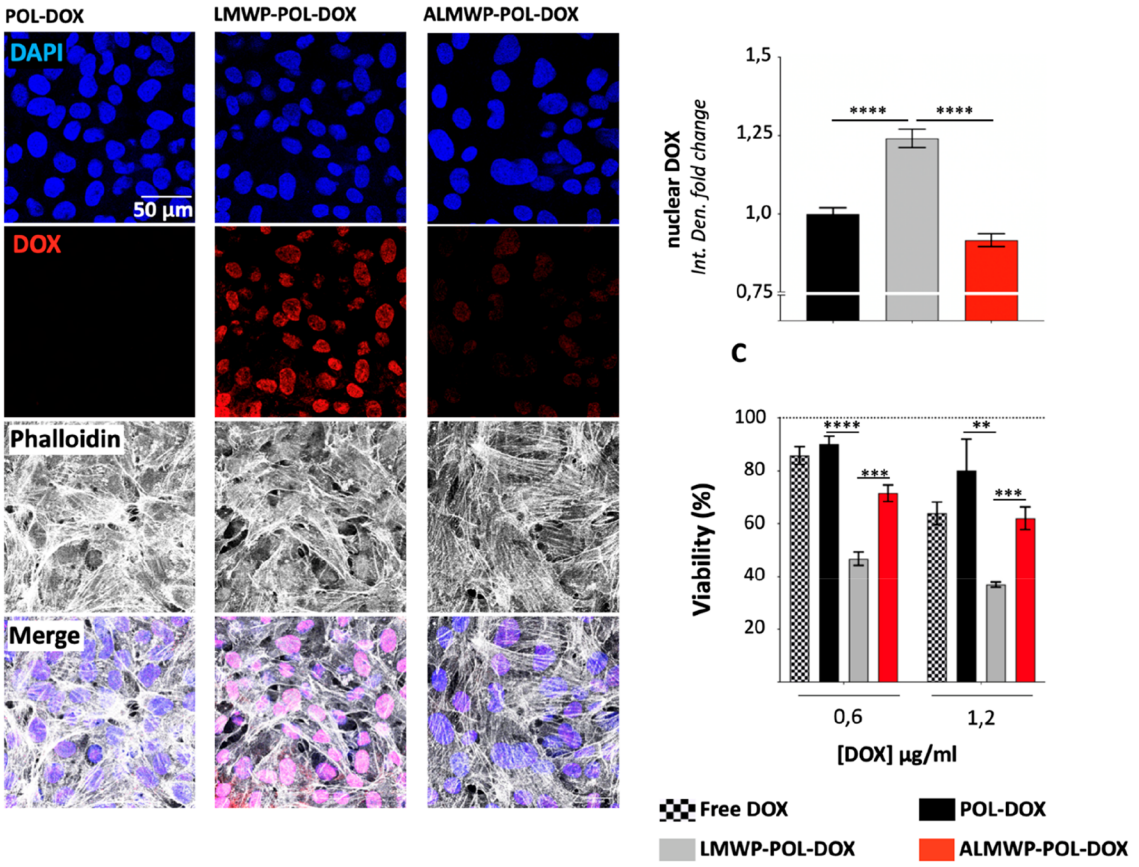

Figure 8. Uptake and viability of hCMEC/d3 endothelial MMP2-negative cells. (A) Representative confocal images of human endothelial cells (hCMEC/d3) after 5 h incubation with indicated POL-DOX nanovectors, [DOX] 1.2 μg/mL. In blue is the Hoechst signal for nucleus detection and in white is Phalloidin for cell body detection. (B) Nuclear DOX quantification expressed as integrated density (Int. Den) ± SE in cells incubated with POL-DOX nanovectors as indicated (6 h, [DOX] 1.2 μg/mL). At least 300 cells per condition were analyzed. (C) Cell viability detected by MTT assay after 24 h incubation with the indicated nanovectors at [DOX] of 0.6 μg/mL. Values are expressed as mean percentage survival (for replicates ± SE) normalized to corresponding untreated cells. Pairwise comparison was performed by Student's t test. $^{**}P < 0.01$, $^{***}P < 0.001$, $^{****}P < 0.0001$.

ICH003 cells indicating a MMP2-dependent ALMWP-POL-DOX (Figure 6C and D).

These results suggest that star comb-like PCL-PEG copolymer can effectively retain DOX into the nanovector core and that the activable peptide can be cleaved by the MMP2 from GBM cells. The MMP2-cleavage of the ALMWP peptide exposed the protamine-based CPP to plasma membranes, allowing POL-DOX nanovectors enter the cells. The corresponding level of MMP2 activity and ALMWP-POL-DOX cellular uptake supported the crucial involvement of the MMP2 enzymatic activity in the activation of the ALMWP nanovectors.

ALMWP-DOX-PCL Affects Cell Viability in a Dose-and Time-Dependent Manner. To verify whether encapsulated DOX was functional and ALMWP-nanovectors could thus be exploited to target tumor cells, cell viability was evaluated in the presence/absence of DOX-loaded nanovectors. ICH001, ICH003, and ICH013 cells were incubated with peptide-free nanovectors (POL-DOX) and conjugated with either the LMWP peptide with penetrating properties (LMWP-POL-DOX) or the AMLWP peptide conferring MMP2 specificity (AMLWP-POL-DOX).

As expected, no/lower toxicity was observed in the presence of the untargeted POL-DOX nanovector in line with its low level of cellular uptake observed in all the cell lines analyzed. Significantly lower cell viability was instead observed after LMWP- and ALMWP-POL-DOX incubation with an equal DOX concentration (0.6 μg/mL), in accordance with the high grade of cell permeability associated with the CPP-functionalized LMWP-nanovector, and with the MMP protease activity of GBM cellswhich induced ALMWP activation (Figure 7A).

Interestingly, while ICH001 and ICH003 cells showed a similar level of cytotoxicity when incubated with LMWP- and ALMWP-POL-DOX nanovectors, ICH013 cells displayed the most sensible response to ALMWP-POL-DOX, displaying a 49% reduction compared to LMWP-POL-DOX. This observation, which is consistent with the ICH013 cells having higher MMP2 enzymatic activity (Figure 6D), enforced the observations showing significantly higher ALMWP-POL-DOX cellular uptake in these cells (Figure 6C).

With a doubled DOX concentration (1.2 μg/mL), ALMWP-POL-DOX cytotoxicity increased, indicating a dose-dependent, and thus active, mechanism of nanovector activation. Moreover, in ICH003 and ICH013, ALMWP nanovectors induced a consistent and significant time-dependent reduction of cell viability (Figure 7B).

MMP2 Is Required to Elicit ALMWP-DOX-PCL Antitumor Activity. Human endothelial cells (hCMEC/d3) not expressing MMP2 (Figure S5, Supporting Information.) were used to validate the targeted strategy based on ALMWP

https://doi.org/10.1021/acsapm.2c00897
ACS Appl. Polym. Mater. 2022, 4, 8043−8056

peptide cleavage as well as to assay nanovector cytotoxicity to nontumoral cells. Unlike GBM cells, endothelial cells showed the highest DOX uptake, evaluated by confocal microscopy, upon exposure to the LMWP-POL-DOX nanovectors, while ALMWP-POL-DOX uptake was significantly lower and equivalent to that of the untargeted POL-DOX (Figure 8A and B). In line with the low degree of cellular uptake, the endothelial cells showed 90% and 72% survival upon exposure to untargeted POL-DOX and ALMWP-POL-DOX nanovectors, respectively. The most toxic nanovector resulted in CPP-decorated LMWP-POL-DOX (Figure 8C). Interestingly, the peak of cytotoxicity was obtained by incubating hCMEC/d3 cells with CPP-conjugated LMWP-POL-DOXO, indicating the ability of CPP decoration to overcome free-DOX resistance of brain endothelial cells mediated by the efflux mechanisms of multidrug resistance proteins.[55] In line with the low degree of cellular uptake, the endothelial cells showed 90% and 72% survival upon exposure to untargeted POL-DOXO and ALMWP-POL-DOXO nanovectors, respectively (Figure 8C). These results strongly support MMP2 involvement in the ALMWP-POL-DOX nanovector activation that led to the generation of the LMWP-POL-DOX penetrating nanovector.

CONCLUSION

In this study, we developed DOX-loaded polymer NPs based on PEG-PCL copolymers with a complex macromolecular architecture. When compared with the linear and 4-arm topology, the 4-arm brush block copolymers were the most suitable for DOX nanoencapsulation, since the resulting nanoparticles showed the best performance in terms of encapsulation efficiency and particle stability.

The occasional occurrence of the activating conditions in normal tissues supports the development of MMP-activable strategies. Indeed, we verified and confirmed the cytotoxicity of DOX-loaded nanocarriers conjugated with a low molecular weight protamine CPP peptide coupled to an MMP-activable peptide sequence (ALMWP) on MMP2-producing GBM cells. Conversely, no detrimental effects were observed in MMP2-negative endothelial cells. As MMP activity level determines the success of the activable nanocarrier, the link of a peptide with cell penetrating properties to a MMPs-sensitive sequence can be considered a promising tumor-targeting strategy.

The advantages of using MMP-activable CPP-functionalized nanocarriers to tackle tumors consists of the possibility to simultaneously improve specificity and cell penetrance, thus limiting off-target effects. The multiple and nonselective mechanisms of cellular entrance engaged by CPPs to drive the cargo inside the cells make them a powerful and efficient tool to target not only tumoral cells but also the surrounding microenvironment.

It has been recently described that when encapsulated DOX successfully crosses the blood-brain barrier and reaches GBM cells, it can efficiently lead to apoptosis and tumor regression.[56] Therefore, despite different chemotherapeutics that can be considered for nanoencapsulation, ALMWP-POL-DOX nanocarriers may represent a valid alternative also for GBM.

ASSOCIATED CONTENT

Supporting Information

The Supporting Information is available free of charge at https://pubs.acs.org/doi/10.1021/acsapm.2c00897.

Kinetic plot and SEC chromatograms, ^{1}H NMR spectra, TEM images, Western blot analysis (PDF)

AUTHOR INFORMATION

Corresponding Authors

Francesco Cellesi − *Department of Chemistry, Materials and Chemical Engineering "G. Natta", Politecnico di Milano, Milano 20131, Italy;* orcid.org/0000-0001-6106-9317; Phone: +39-02-23993099; Email: francesco.cellesi@polimi.it

Lorena Passoni − *Laboratory of Pharmacology and Brain Pathology, IRCCS Humanitas Research Hospital, 20089 Rozzano, Milano, Italy;* orcid.org/0000-0002-9468-2166; Phone: +39-02-82245135; Email: lorena.passoni@humanitasresearch.it

Authors

Wanda Celentano − *Department of Chemistry, Materials and Chemical Engineering "G. Natta", Politecnico di Milano, Milano 20131, Italy; Laboratory of Pharmacology and Brain Pathology, IRCCS Humanitas Research Hospital, 20089 Rozzano, Milano, Italy*

Marco Pizzocri − *Laboratory of Pharmacology and Brain Pathology, IRCCS Humanitas Research Hospital, 20089 Rozzano, Milano, Italy*

Filippo Moncalvo − *Department of Chemistry, Materials and Chemical Engineering "G. Natta", Politecnico di Milano, Milano 20131, Italy*

Federico Pessina − *Neurosurgery Department, IRCCS Humanitas Research Hospital, 20089 Rozzano, Milano, Italy; Department of Biomedical Sciences, Humanitas University, 20072 Pieve Emanuele, Milan, Italy*

Michela Matteoli − *Laboratory of Pharmacology and Brain Pathology, IRCCS Humanitas Research Hospital, 20089 Rozzano, Milano, Italy; Department of Biomedical Sciences, Humanitas University, 20072 Pieve Emanuele, Milan, Italy*

Complete contact information is available at: https://pubs.acs.org/10.1021/acsapm.2c00897

Author Contributions

#W.C., M.P., F.C., and L.P. equally contributed.

Notes

The authors declare no competing financial interest.

ACKNOWLEDGMENTS

This work was supported by Fondazione AIRC per la Ricerca sul Cancro (IG 18851 to M.M.), Fondazione Umberto Veronesi (grant to L.P. and fellowships to M.P.), and by Regione Lombardia (POR FESR 2014-2020) within the framework of the NEWMED project (ID 1175999). We thank Giuditta Magnifico and Giulia Giampietro (Master students at the Department of Chemistry, Materials and Chemical Engineering, Politecnico di Milano, Italy) for their support with polymer synthesis and characterization.

REFERENCES

(1) Diao, Y.-Y.; Li, H.-Y.; Fu, Y.-H.; Han, M.; Hu, Y.-L.; Jiang, H.-L.; Tsutsumi, Y.; Wei, Q.-C.; Chen, D.-W.; Gao, J.-Q. Doxorubicin-loaded PEG-PCL copolymer micelles enhance cytotoxicity and intracellular accumulation of doxorubicin in adriamycin-resistant tumor cells. *Int. J. Nanomedicine* **2011**, *6*, 1955−1962.

(2) Reshma, J.; Jinu, G.; Franklin, J. Brief Outlook on Polymeric Nanoparticles, Micelles, Niosomes, Hydrogels and Liposomes:

Preparative Methods and Action. *ChemistrySelect* **2022**, *7*, e202104045.
(3) Conte, C.; d'Angelo, I.; Miro, A.; Ungaro, F.; Quaglia, F. PEGylated Polyester-Based Nanoncologicals. *Current Topics in Medicinal Chemistry* **2014**, *14*, 1097−1114.
(4) Yi, Y.; Lin, G.; Chen, S. Y.; Liu, J.; Zhang, H. P.; Mi, P. Polyester micelles for drug delivery and cancer theranostics: Current achievements, progresses and future perspectives. *Materials Science & Engineering C-Materials for Biological Applications* **2018**, *83*, 218−232.
(5) Liu, Z.; Ji, X.; He, D.; Zhang, R.; Liu, Q.; Xin, T. Nanoscale Drug Delivery Systems in Glioblastoma. *Nanoscale Res. Lett.* **2022**, *17*, 27.
(6) Niculescu, A. G.; Grumezescu, A. M. Novel Tumor-Targeting Nanoparticles for Cancer Treatment-A Review. *Int. J. Mol. Sci.* **2022**, 5253.
(7) Hou, Z.; Zhou, W.; Guo, X.; Zhong, R.; Wang, A.; Li, J.; Cen, Y.; You, C.; Tan, H.; Tian, M. Poly(ε-Caprolactone)-Methoxypolyethylene Glycol (PCL-MPEG)-Based Micelles for Drug-Delivery: The Effect of PCL Chain Length on Blood Components, Phagocytosis, and Biodistribution. *Int. J. Nanomedicine* **2022**, *17*, 1613−1632.
(8) Grossen, P.; Witzigmann, D.; Sieber, S.; Huwyler, J. PEG-PCL-based nanomedicines: A biodegradable drug delivery system and its application. *J. Controlled Release* **2017**, *260*, 46−60.
(9) Moncalvo, F.; Martinez Espinoza, M. I.; Cellesi, F. Nanosized Delivery Systems for Therapeutic Proteins: Clinically Validated Technologies and Advanced Development Strategies. *Frontiers in Bioengineering and Biotechnology* **2020**, 8.
(10) Jokerst, J. V.; Lobovkina, T.; Zare, R. N.; Gambhir, S. S. Nanoparticle PEGylation for imaging and therapy. *Nanomedicine (Lond)* **2011**, *6*, 715−728.
(11) Huang, Y.; Gao, H.; Gou, M.; Ye, H.; Liu, Y.; Gao, Y.; Peng, F.; Qian, Z.; Cen, X.; Zhao, Y. Acute toxicity and genotoxicity studies on poly(ε-caprolactone)-poly(ethylene glycol)-poly(ε-caprolactone) nanomaterials. *Mutation Research/Genetic Toxicology and Environmental Mutagenesis* **2010**, *696*, 101−106.
(12) Bruni, R.; Possenti, P.; Bordignon, C.; Li, M.; Ordanini, S.; Messa, P.; Rastaldi, M. P.; Cellesi, F. Ultrasmall polymeric nanocarriers for drug delivery to podocytes in kidney glomerulus. *J. Controlled Release* **2017**, *255*, 94−107.
(13) Zhang, L.; Chen, Z.; Wang, H.; Wu, S.; Zhao, K.; Sun, H.; Kong, D.; Wang, C.; Leng, X.; Zhu, D. Preparation and evaluation of PCL−PEG−PCL polymeric nanoparticles for doxorubicin delivery against breast cancer. *RSC Adv.* **2016**, *6*, 54727−54737.
(14) Avramović, N.; Mandić, B.; Savić-Radojević, A.; Simić, T. Polymeric Nanocarriers of Drug Delivery Systems in Cancer Therapy. *Pharmaceutics* **2020**, *12*, 298.
(15) Kakkar, A.; Traverso, G.; Farokhzad, O. C.; Weissleder, R.; Langer, R. Evolution of macromolecular complexity in drug delivery systems. *Nat. Rev. Chem.* **2017**, *1*, 63.
(16) Lotocki, V.; Kakkar, A. Miktoarm Star Polymers: Branched Architectures in Drug Delivery. *Pharmaceutics* **2020**, *12*, 827.
(17) Ordanini, S.; Cellesi, F. Complex Polymeric Architectures Self-Assembling in Unimolecular Micelles: Preparation, Characterization and Drug Nanoencapsulation. *Pharmaceutics* **2018**, *10*, 209.
(18) Manjili, H. K.; Sharafi, A.; Danafar, H.; Hosseini, M.; Ramazani, A.; Ghasemi, M. H. Poly(caprolactone)−poly(ethylene glycol)−poly(caprolactone) (PCL−PEG−PCL) nanoparticles: a valuable and efficient system for in vitro and in vivo delivery of curcumin. *RSC Adv.* **2016**, *6*, 14403−14415.
(19) Celentano, W.; Ordanini, S.; Bruni, R.; Marocco, L.; Medaglia, P.; Rossi, A.; Buzzaccaro, S.; Cellesi, F. Complex poly(ε-caprolactone)/poly(ethylene glycol) copolymer architectures and their effects on nanoparticle self-assembly and drug nanoencapsulation. *Eur. Polym. J.* **2021**, *144*, 110226.
(20) Ordanini, S.; Celentano, W.; Bernardi, A.; Cellesi, F. Mannosylated brush copolymers based on poly(ethylene glycol) and poly(epsilon-caprolactone) as multivalent lectin-binding nanomaterials. *Beilstein Journal of Nanotechnology* **2019**, *10*, 2192−2206.
(21) Gu, G.; Xia, H.; Hu, Q.; Liu, Z.; Jiang, M.; Kang, T.; Miao, D.; Tu, Y.; Pang, Z.; Song, Q.; Yao, L.; Chen, H.; Gao, X.; Chen, J. PEG-co-PCL nanoparticles modified with MMP-2/9 activatable low molecular weight protamine for enhanced targeted glioblastoma therapy. *Biomaterials* **2013**, *34*, 196−208.
(22) White, B. D.; Duan, C.; Townley, H. E. Nanoparticle Activation Methods in Cancer Treatment. *Biomolecules* **2019**, *9*, 202.
(23) Kamaly, N.; Xiao, Z.; Valencia, P. M.; Radovic-Moreno, A. F.; Farokhzad, O. C. Targeted polymeric therapeutic nanoparticles: design, development and clinical translation. *Chem. Soc. Rev.* **2012**, *41*, 2971−3010.
(24) Wei, G.; Wang, Y.; Huang, X.; Yang, G.; Zhao, J.; Zhou, S. Enhancing the Accumulation of Polymer Micelles by Selectively Dilating Tumor Blood Vessels with NO for Highly Effective Cancer Treatment. *Adv. Healthcare Mater.* **2018**, *7*, 1801094.
(25) de la Cruz-López, K. G.; Castro-Muñoz, L. J.; Reyes-Hernández, D. O.; García-Carrancá, A.; Manzo-Merino, J. Lactate in the Regulation of Tumor Microenvironment and Therapeutic Approaches. *Frontiers in Oncology* **2019**, *9*, 1143.
(26) Piasentin, N.; Milotti, E.; Chignola, R. The control of acidity in tumor cells: a biophysical model. *Sci. Rep.* **2020**, *10*, 13613.
(27) Gonzalez-Avila, G.; Sommer, B.; García-Hernández, A. A.; Ramos, C.Matrix Metalloproteinases' Role in Tumor Microenvironment. In *Tumor Microenvironment: Extracellular Matrix Components − Part A*; Birbrair, A., Ed.; Springer International Publishing: Cham, 2020; pp 97−131.
(28) Piperigkou, Z.; Kyriakopoulou, K.; Koutsakis, C.; Mastronikolis, S.; Karamanos, N. K. Key Matrix Remodeling Enzymes: Functions and Targeting in Cancer. *Cancers* **2021**, *13*, 1441.
(29) Damsky, W. E.; Rosenbaum, L. E.; Bosenberg, M. Decoding Melanoma Metastasis. *Cancers* **2011**, *3*, 126.
(30) Berman, A. T.; Thukral, A. D.; Hwang, W. T.; Solin, L. J.; Vapiwala, N. Incidence and patterns of distant metastases for patients with early-stage breast cancer after breast conservation treatment. *Clin Breast Cancer* **2013**, *13*, 88−94.
(31) Milovanovic, I. S.; Stjepanovic, M.; Mitrovic, D. Distribution patterns of the metastases of the lung carcinoma in relation to histological type of the primary tumor: An autopsy study. *Ann. Thorac Med.* **2017**, *12*, 191−198.
(32) Yu, C.-F.; Chen, F.-H.; Lu, M.-H.; Hong, J.-H.; Chiang, C.-S. Dual roles of tumour cells-derived matrix metalloproteinase 2 on brain tumour growth and invasion. *Br. J. Cancer* **2017**, *117*, 1828−1836.
(33) Nagel, G.; Sousa-Herves, A.; Wedepohl, S.; Calderón, M. Matrix Metalloproteinase-sensitive Multistage Nanogels Promote Drug Transport in 3D Tumor Model. *Theranostics* **2020**, *10*, 91−108.
(34) Chu, S.; Shi, X.; Tian, Y.; Gao, F. pH-Responsive Polymer Nanomaterials for Tumor Therapy. *Frontiers in Oncology* **2022**, *12*, 855019.
(35) van Duijnhoven, S. M. J.; Robillard, M. S.; Nicolay, K.; Grüll, H. Tumor Targeting of MMP-2/9 Activatable Cell-Penetrating Imaging Probes Is Caused by Tumor-Independent Activation. *J. Nucl. Med.* **2011**, *52*, 279.
(36) Xia, H.; Gu, G.; Hu, Q.; Liu, Z.; Jiang, M.; Kang, T.; Miao, D.; Song, Q.; Yao, L.; Tu, Y.; Chen, H.; Gao, X.; Chen, J. Activatable Cell Penetrating Peptide-Conjugated Nanoparticles with Enhanced Permeability for Site-Specific Targeting Delivery of Anticancer Drug. *Bioconjugate Chem.* **2013**, *24*, 419−430.
(37) He, H.; Ye, J.; Liu, E.; Liang, Q.; Liu, Q.; Yang, V. C. Low molecular weight protamine (LMWP): a nontoxic protamine substitute and an effective cell-penetrating peptide. *J. Controlled Release* **2014**, *193*, 63−73.
(38) Xia, H.; Gao, X.; Gu, G.; Liu, Z.; Zeng, N.; Hu, Q.; Song, Q.; Yao, L.; Pang, Z.; Jiang, X.; Chen, J.; Chen, H. Low molecular weight protamine-functionalized nanoparticles for drug delivery to the brain after intranasal administration. *Biomaterials* **2011**, *32*, 9888−9898.
(39) Reissmann, S. Cell penetration: scope and limitations by the application of cell-penetrating peptides. *Journal of Peptide Science* **2014**, *20*, 760−784.
(40) Aguilera, T. A.; Olson, E. S.; Timmers, M. M.; Jiang, T.; Tsien, R. Y. Systemic in vivo distribution of activatable cell penetrating

peptides is superior to that of cell penetrating peptides. *Integr Biol. (Camb)* **2009**, *1*, 371−381.
(41) Jiang, T.; Olson, E. S.; Nguyen, Q. T.; Roy, M.; Jennings, P. A.; Tsien, R. Y. Tumor imaging by means of proteolytic activation of cell-penetrating peptides. *Proc. Natl. Acad. Sci. U.S.A.* **2004**, *101*, 17867−17872.
(42) Olson, E. S.; Aguilera, T. A.; Jiang, T.; Ellies, L. G.; Nguyen, Q. T.; Wong, E. H.; Gross, L. A.; Tsien, R. Y. In vivo characterization of activatable cell penetrating peptides for targeting protease activity in cancer. *Integr Biol. (Camb)* **2009**, *1*, 382−393.
(43) Gritti, A.; Parati, E. A.; Cova, L.; Frolichsthal, P.; Galli, R.; Wanke, E.; Faravelli, L.; Morassutti, D. J.; Roisen, F.; Nickel, D. D.; Vescovi, A. L. Multipotential stem cells from the adult mouse brain proliferate and self-renew in response to basic fibroblast growth factor. *J. Neurosci.* **1996**, *16*, 1091.
(44) Frankowski, H.; Gu, Y. H.; Heo, J. H.; Milner, R.; Del Zoppo, G. J. Use of gel zymography to examine matrix metalloproteinase (gelatinase) expression in brain tissue or in primary glial cultures. *Methods Mol. Biol.* **2012**, *814*, 221−33.
(45) Celentano, W.; Battistella, J.; Silvestri, I. P.; Bruni, R.; Huang, X.; Li, M.; Messa, P.; Ordanini, S.; Cellesi, F. Engineered polyester-PEG nanoparticles prepared through a "grafting through" strategy and post-functionalization via Michael type addition. *React. Funct. Polym.* **2018**, *131*, 164−173.
(46) Ragupathy, L.; Millar, D. G.; Tirelli, N.; Cellesi, F. An Orthogonal Click-Chemistry Approach to Design Poly(glycerol monomethacrylate)-based Nanomaterials for Controlled Immunostimulation. *Macromol. Biosci.* **2014**, *14*, 1528−1538.
(47) Doncom, K. E. B.; Blackman, L. D.; Wright, D. B.; Gibson, M. I.; O'Reilly, R. K. Dispersity effects in polymer self-assemblies: a matter of hierarchical control. *Chem. Soc. Rev.* **2017**, *46*, 4119−4134.
(48) Le Fer, G.; Le Coeur, C.; Guigner, J.-M.; Amiel, C.; Volet, G. Amphiphilic diblock and triblock copolymers based on poly(2-methyl-2-oxazoline) and poly(D,L-lactide): Synthesis, physicochemical characterizations and self-assembly properties. *Polymer* **2019**, *171*, 149−160.
(49) Zhu, Z. Flash nanoprecipitation: prediction and enhancement of particle stability via drug structure. *Mol. Pharmaceutics* **2014**, *11*, 776−786.
(50) Martwong, E.; Tran, Y. Lower Critical Solution Temperature Phase Transition of Poly(PEGMA) Hydrogel Thin Films. *Langmuir* **2021**, *37*, 8585−8593.
(51) Ward, M. A.; Georgiou, T. K. Thermoresponsive Polymers for Biomedical Applications. *Polymers* **2011**, *3*, 1215−1242.
(52) Cuong, N.-V.; Jiang, J.-L.; Li, Y.-L.; Chen, J.-R.; Jwo, S.-C.; Hsieh, M.-F. Doxorubicin-Loaded PEG-PCL-PEG Micelle Using Xenograft Model of Nude Mice: Effect of Multiple Administration of Micelle on the Suppression of Human Breast Cancer. *Cancers* **2011**, *3*, 61−78.
(53) Colombo, C.; Li, M.; Watanabe, S.; Messa, P.; Edefonti, A.; Montini, G.; Moscatelli, D.; Rastaldi, M. P.; Cellesi, F. Polymer Nanoparticle Engineering for Podocyte Repair: From in Vitro Models to New Nanotherapeutics in Kidney Diseases. *ACS Omega* **2017**, *2*, 599−610.
(54) Wang, J.; Xing, X.; Fang, X.; Zhou, C.; Huang, F.; Wu, Z.; Lou, J.; Liang, W. Cationic amphiphilic drugs self-assemble to the core−shell interface of PEGylated phospholipid micelles and stabilize micellar structure. *Philosophical Transactions of the Royal Society A: Mathematical, Physical and Engineering Sciences* **2013**, *371*, 20120309.
(55) Han, B.; Xie, W.; Zhang, Y.; Zhou, S.; Yang, J.; Wang, R.; Sun, Y.; Wang, X.; Xu, J.; Chen, D.; Wang, Y.; Lu, J.; Ning, F.; Shen, F.; Liu, M.; Cai, H.; Xin, H.; Lu, W.; Zhang, X. The influx/efflux mechanisms of d-peptide ligand of nAChRs across the blood-brain barrier and its therapeutic value in treating glioma. *J. Controlled Release* **2020**, *327*, 384−396.
(56) Pizzocri, M.; Re, F.; Stanzani, E.; Formicola, B.; Tamborini, M.; Lauranzano, E.; Ungaro, F.; Rodighiero, S.; Francolini, M.; Gregori, M.; Perin, A.; DiMeco, F.; Masserini, M.; Matteoli, M.; Passoni, L. Radiation and adjuvant drug-loaded liposomes target glioblastoma stem cells and trigger in-situ immune response. *Neuro-Oncology Advances* **2021**, *3*, vdab076.

https://doi.org/10.1021/acsapm.2c00897
ACS Appl. Polym. Mater. 2022, 4, 8043−8056